ELSEVIER

NeuroImage

www.elsevier.com/locate/ynimg
NeuroImage 25 (2005) 701–707

Simultaneous recording of task-induced changes in blood oxygenation, volume, and flow using diffuse optical imaging and arterial spin-labeling MRI

R.D. Hoge,[a,*] M.A. Franceschini,[a] R.J.M. Covolan,[b] T. Huppert,[a] J.B. Mandeville,[a] and D.A. Boas[a]

[a]*Athinoula A. Martinos Center for Biomedical Imaging, Massachusetts General Hospital, Building 149 13th Street, Charlestown, MA 02129, USA*
[b]*Instituto de Física Gleb Wataghin, Universidade Estadual de Campinas, Unicamp, 13083-970 Campinas SP Brazil*

Received 22 March 2004; revised 7 December 2004; accepted 10 December 2004
Available online 17 February 2005

Increased neural activity in brain tissue is accompanied by an array of supporting physiological processes, including increases in blood flow and the rates at which glucose and oxygen are consumed. These responses lead to secondary effects such as alterations in blood oxygenation and blood volume, and are ultimately the primary determinants of the amplitude and temporal signature of the blood oxygenation level-dependent (BOLD) signal used prevalently to map brain function. We have performed experiments using a combination of optical and MRI-based imaging methods to develop a more comprehensive picture of the physiological events accompanying activation of primary motor cortex during a finger apposition task. Temporal profiles for changes in tissue hemoglobin concentrations were qualitatively similar to those observed for MRI-based flow and oxygenation signals. Quantitative analysis of these signals revealed peak changes of +16 ± 2% for HbO, −13 ± 2% for HbR, +8 ± 3% for total Hb, +83 ± 9% for cerebral blood flow, and +1.4 ± 0.1% for the BOLD MRI signal. A mass balance model was used to estimate the change in rate of oxidative metabolism implied by the optical and flow measurements, leading to a computed value of +47 ± 5%. It should be noted that the optical and MRI observations may in general reflect changes over different volumes of tissue. The ratio of fractional changes in oxidative metabolism to fractional change in blood flow was found to be 0.56 ± 0.08, in general agreement with previous studies of flow–metabolism coupling.

Keywords: Optical imaging; Functional MRI; Hemodynamics; Arterial spin-labeling; Metabolism

Introduction

Diffuse optical imaging (DOI) and arterial spin-labeling with magnetic resonance imaging (ASLMRI) offer complementary views of the physiological events accompanying brain activation. DOI (Boas et al., 2003; Villringer and Chance, 1997) allows recording of changes in the concentration of oxygenated and deoxygenated hemoglobin, while ASL-MRI (Kim, 1995) depicts changes in perfusion during activation. Oxyhemoglobin (HbO) and deoxyhemoglobin (HbR) are chromophores that exhibit markedly different absorption spectra in the near-infrared region (Sfareni et al., 1997; Wray et al., 1988), for wavelengths typically in the range 650–950 nm. Since water absorption is weak in this region and these hemoglobin species appear in low but detectable concentrations (<100 μM), light can still be detected after passing through the skull and several centimeters of brain tissue (Gratton et al., 1994; Jobsis, 1977), opening up an "optical window" for noninvasive assessment of hemodynamic changes. In addition, the sum of these hemoglobin components provides a measure of total hemoglobin concentration [HbT] and an estimate of blood volume.

Arterial spin-labeling, in turn, uses magnetically labeled blood as an endogenous tracer allowing for quantitative perfusion imaging. Subsequent diffusion of labeled blood water into tissue alters the local magnetization, leading to a component of the MRI signal that is dependent on the local rate of blood flow (Detre and Alsop, 2000).

The prevalent method used currently for functional brain imaging is based on the blood oxygen level-dependence (BOLD) of T_2^*-weighted MRI signals (Kwong et al., 1992; Ogawa et al., 1992) due to the relatively high sensitivity of this method as well as its simplicity. A limitation of BOLD methods is that they are physiologically ambiguous, depending jointly on changes in blood flow, oxidative metabolism, and blood volume. Arterial spin-labeling offers the advantage of depicting a specific physiological variable (blood flow rate), but suffers from reduced sensitivity compared with BOLD due to the small amplitude of the flow-related MRI signal that can be achieved with currently available labeling methods.

The simultaneous combination of DOI and ASL-MRI during brain activation experiments creates the possibility for inves-

* Corresponding author. Fax: +1 617 726 7422.
E-mail address: rhoge@nmr.mgh.harvard.edu (R.D. Hoge).
Available online on ScienceDirect (www.sciencedirect.com).

1053-8119/$ - see front matter © 2004 Published by Elsevier Inc.
doi:10.1016/j.neuroimage.2004.12.032

tigating not only the hemodynamic aspects of brain activation, but also associated metabolic variables such as oxygen extraction fraction (OEF) and cerebral metabolic rate for oxygen consumption ($CMRO_2$) (Davis et al., 1998; Kim and Ugurbil, 1997). By providing a more comprehensive set of physical observables, this multimodal approach also allows elimination of some of the assumptions on which methods based purely on MRI or optical detection have relied in the past. In particular, it removes the need to assume an empirically derived flow–volume coupling relationship such as the association identified by Grubb et al. (1974).

Difficulties in the present method include the inability of the optical method to provide quantitative measures of baseline hemoglobin concentrations, requiring use of baseline concentrations obtained from published literature, and the fact that the optical and MR observations may reflect responses in different volumes of tissue.

Methods

Subjects and protocol

Seven right-handed volunteers underwent simultaneous diffuse optical recording and functional MR scanning. All procedures were examined and approved by the Institutional Review Board at the Massachusetts General Hospital, where the experiments were carried out. All subjects gave their written informed consent.

The experimental manipulation consisted of a self-paced finger apposition task with the dominant (right) hand during 12 trials of 20-s duration each at 80% of the subject's maximal rate. This subjective pacing directive was given to allow rapid finger movements, and thus large amplitude changes, without body motion that was observed when subjects attempted maximal rates. Finger motion was tracked using an optical probe affixed to the thumb and was typically observed to be in the range from 2 to 3 Hz.

Each functional scanning run began with a baseline interval of 40 s, followed by three cycles of a 20-s task followed by 60 s of baseline. Total run duration was 280 s. Each subject performed four runs, with three trials in each run. DOI and ASL signals were recorded simultaneously throughout all runs.

To assess subject compliance with the task, a fiber optic sensor was placed between the thumb and fore-finger of the subject's dominant (tapping) hand. Unfortunately, due to technical reasons, this information did not give a reliable measure of subject tapping frequency.

Diffuse optical measurements

During scanning runs, DOI was performed using a multi-channel continuous wave system (Cw4) (Franceschini et al., 2001). This instrument was developed jointly between the Photon Migration Lab at the Athinoula A. Martinos Center for Biomedical Imaging/Massachusetts General Hospital and TechEn Inc. (Milford, MA). The imager has 18 lasers–9 lasers at 690 nm and 9 at 830 nm–and 16 detectors of which only 4 source positions (2 wavelengths each) and 8 detectors were used in this experiment. Laser wavelengths were chosen to minimize cross-talk between the two hemoglobin species at 690 nm and 830 nm (18 mW and 7 mW, respectively) (Strangman et al., 2003). Each laser is amplitude modulated at a unique carrier between 4 and 7.4 kHz in approximately 200 Hz steps. This allows for laser source distinguishably by demodulation against the known carrier frequencies on each detector channel in post-processing. For detectors, the imager employs 16 avalanche photodiodes (APD's, Hamamatsu C5460-01), each of which is digitized at approximately 40 kHz.

The optical probe array was made from flexible plastic strips with plastic caps inserted in it to hold the ends of the 10 m source/detector fiber optic bundles. The probe array consisted of one column containing four light sources flanked by two columns each containing four detector elements, with these twelve elements arranged in a rectangular grid pattern with 2.9 cm separation between nearest neighbor source–detector pairs as shown in Fig. 1. The probe array was secured to the subject's head over the contra-lateral primary motor cortex (M1) via Velcro straps and foam padding. Positioning was verified prior to functional data acquisition using T1-weighted MR scans based on MR-visible fiducial markers attached to the probe. The fiber optics were run through the magnet bore to the back-end room of the scanner where they were connected to the optical instrument.

Following acquisition, the optical data are first demodulated against the laser carrier frequencies to separate source detector pairs

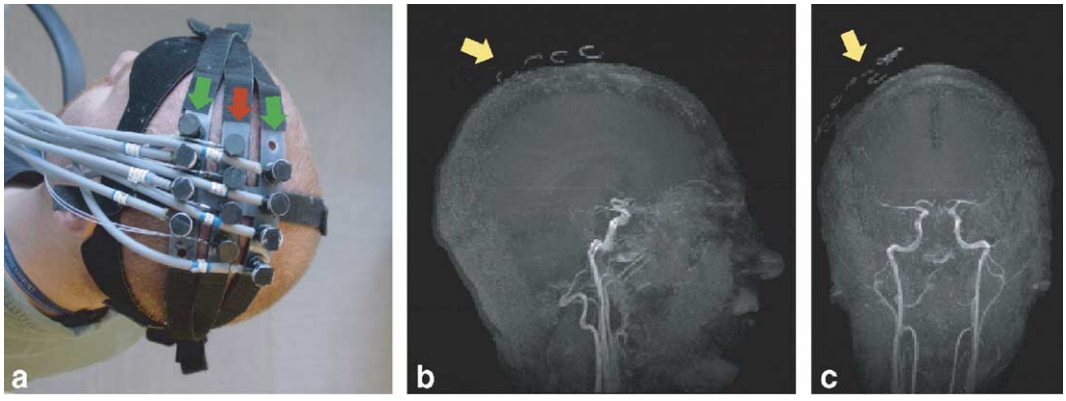

Fig. 1. Optical source detector array. (a) Array mounted over the left motor cortex of subject. The central column of four black circles is the set of four light sources (red arrow), flanked by two columns each containing four detectors (green arrow). (b and c) Maximum intensity projection of 3D MPRAGE scan showing MR-visible markers affixed to sources and detectors (yellow arrows) in sagittal and coronal planes.

and then low-pass filtered and data were downsampled to 10 Hz. The data are then further processed using a custom-written Matlab analysis program. The signals for the two wavelengths are first band pass filtered with a pass band of 0.0167–0.5 Hz before being converted to hemoglobin concentrations using the modified Beer–Lambert equation with a differential path length correction of 6 and a partial volume correction of 50 for both wavelengths. These correction values have been extensively investigated by Strangman et al. (2003) and were chosen to minimize cross-talk between the two hemoglobin species and correct for the DOI partial volume effect. These hemoglobin concentrations were then block averaged to depict the task-related response seen by each of the 14 nearest-neighbor source/detector pairs over all runs. Region of interest averages were then calculated from the average of all source–detector pairs which showed better than $P < 0.05$ significance. Two subjects failed to show any activation with these criteria. Fractional change values were estimated based on assumed baseline concentrations of 25 and 60 μM for HbR and HbO, respectively (Toricelli et al., 2001).

ASL-MRI acquisition

Arterial spin-labeling MRI (ASL) was carried out simultaneously using a 3-T Siemens Allegra MR scanner (Siemens Medical Systems, Erlangen Germany) using PICORE labeling geometry (Wong et al., 1997) with Q2TIPS saturation (Luh et al., 1999) to impose a controlled label duration. A post-label delay of 1400 ms and a label duration of 700 ms were used, with repetition and (gradient) echo times of 2 s and 20 ms, respectively. The PICORE labeling scheme allowed collection of BOLD signals using the control phase of the acquisition. EPI was used to image five 7-mm slices with 3.75-mm in-plane spatial resolution. Structural scans were also performed using a T1-weighted MPRAGE sequence (1 × 1 × 1.33 mm resolution, TR/TE/α = 2.53 s/3.25 ms/7°).

Data analysis

Estimation of flow effects

Flow response amplitudes were estimated using a procedure designed to minimize errors from variations in BOLD signal during the interval between the tag and control phases of the ASL acquisition. First, flow image series were generated by subtracting each negatively labeled tag scan from the immediately subsequent control scan. For each run, effect and standard deviation maps were generated by fitting a linear signal model to each voxel in the flow series. The model consisted of a term representing the three task epochs in the run convolved with a single gamma function (time-to-peak = 5.4 s, width = 5.2 s Worsley and Friston, 1995), plus a third order polynomial. For each subject, the effect and standard deviation maps were input to a mixed effects analysis (target degrees of freedom = 100) to generate a map of t statistic used to identify regions of significant response (Worsley and Friston, 1995). Each t map was thresholded at threshold $P = 0.01$, and then manually edited to remove the ipsilateral primary motor cortex (M1) and the supplementary motor area (SMA). In all subjects, this resulted in a focal region of interest (ROI) positioned on the precentral gyrus and located beneath the source–detector array of the optical apparatus. The average signal within this ROI was then extracted from each original (unsubtracted) EPI series, yielding a signal exhibiting both the task-related response and an oscillation due to the alternation between tag and control in the ASL series (Fig. 2).

Separate linear model fits were then performed on the tag (0,2,4,...) and control (1,3,5,...) points within the ROI signal, with a 2-s shift applied to the time-to-peak of the gamma function used to convolve the response regressor for the control series (to reflect the delay of in the pulse sequence).

The difference between the estimated constant (DC) terms for the tag and control signals was then used as the baseline ASL signal, while the difference between the estimated effect sizes for tag and control was taken as the change in ASL signal. This allowed the fractional change in flow to be computed as follows:

$$\frac{\Delta \mathrm{CBF}}{\mathrm{CBF}_0} = \frac{E_0 - E_1}{\mathrm{DC}_0 - \mathrm{DC}_1} \quad (1)$$

where E_0 and E_1 are the estimated effect sizes for the control and tag signals, respectively, and DC_0 and DC_1 are the respective constant terms estimated for the control and tag signals. Because BOLD signal changes introduce a small multiplicative factor into the difference signal that is not removed by subtraction, the above expression does not completely eliminate BOLD effects from the apparent flow signal. However, because the BOLD factor from this source is very small (typically 2% of the difference signal), it could be safely ignored as it was negligible compared to the much larger measurement noise. This procedure was repeated for each run in each subject and the results averaged to yield an estimate of the flow response for the group.

Computation of OEF and $CMRO_2$

To determine the change in oxidative metabolism implied by the above measurements, a mass balance approach based on

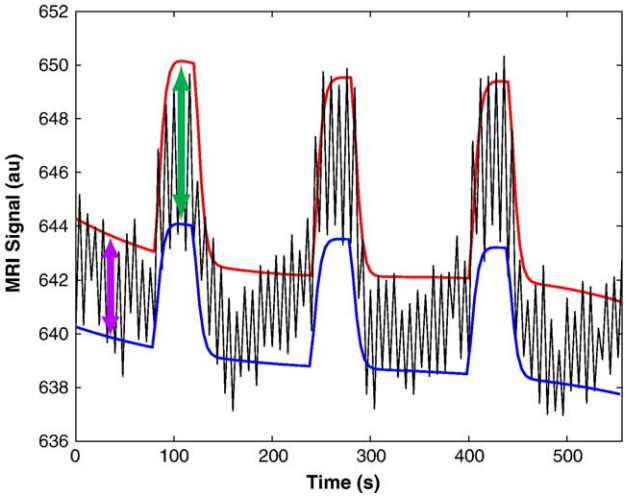

Fig. 2. Linear modeling of the ASL signal. The unsubtracted EPI signal from an ROI in the primary motor cortex is shown in black. Three epochs of the motor task are represented in this plot, which shows data from a single subject. The red curve is a linear model fit using the points from the control phase of the acquisition (points 1,3,5,...) and the blue curve is a separate model fit for the tag points (0,2,4,...). The difference between the baseline (magenta arrow) and activated (green arrow) signal levels was used to estimate the change in blood flow.

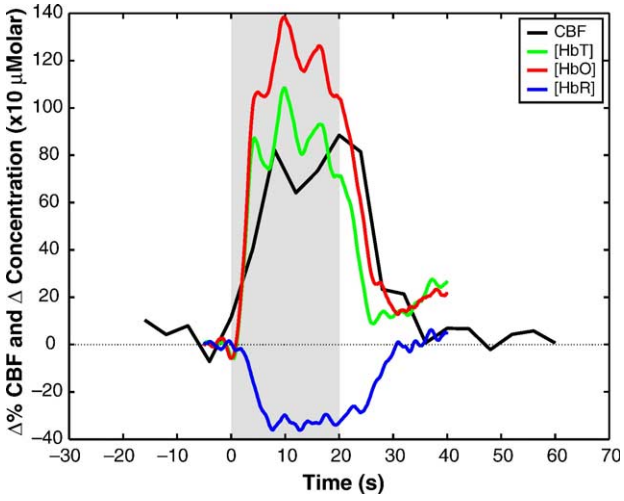

Fig. 3. Plots of change in cerebral blood flow and hemoglobin concentrations. The concentration curves are in units of concentration (×10), using correction factors for path length and partial volume described in the text. The period of task performance is indicated by the shaded background. Cerebral blood flow is shown in units of percent change.

Buxton's balloon model was used (Buxton et al., 1998). The rate of oxidative metabolism, relative to baseline, can be expressed as the product of the relative oxygen extraction fraction and rate of blood flow:

$$\frac{\mathrm{CMR_{O_2}}}{\mathrm{CMR_{O_2}}|_0} = \frac{\mathrm{OEF}}{\mathrm{OEF_0}}\frac{\mathrm{CBF}}{\mathrm{CBF_0}} \tag{2}$$

where $\mathrm{CMR_{O_2}}|_0$, $\mathrm{OEF_0}$, and $\mathrm{CBF_0}$ denote baseline quantities for the relevant variables.

The relative CBF value was available directly from the arterial spin-labeling measurement, while relative OEF was determined from the optical observations using equations adapted from Buxton et al.'s (1998) Eq. (5) in the balloon model article:

$$\frac{\mathrm{OEF}}{\mathrm{OEF_0}} = \frac{q}{v} + \frac{\tau_0}{f_{\mathrm{in}}}\left[\frac{\mathrm{d}q}{\mathrm{d}t} - \frac{q}{v}\frac{\mathrm{d}v}{\mathrm{d}t}\right] \tag{3}$$

where q is the concentration of deoxygenated hemoglobin normalized to baseline, v is the baseline-normalized blood volume, τ_0 is the mean transit time through the venous compartment at rest, and f_{in} is the baseline-normalized flow into the venous compartment. For steady-state observations, the second term is zero because the temporal derivatives vanish. This allows the relative OEF to be expressed as

$$\frac{\mathrm{OEF}}{\mathrm{OEF_0}} = \frac{\left(\frac{PL\ell_{\mathrm{dpf}}\Delta\mathrm{OD}_{690}}{[\mathrm{HbR}]_0}\right)}{\left(\frac{PL\ell_{\mathrm{dpf}}(\Delta\mathrm{OD}_{690}+\Delta\mathrm{OD}_{830})}{[\mathrm{HbT}]_0}\right)} = \frac{\Delta\mathrm{OD}_{690}}{\Delta\mathrm{OD}_{690}+\Delta\mathrm{OD}_{830}}\cdot\frac{[\mathrm{HbT}]_0}{[\mathrm{HbR}]_0} \tag{4}$$

where P is the partial-volume correction factor (50), L is the source-detector separation (3 cm), ℓ_{dpf} is the differential path length correction factor (6) (Strangman et al., 2003), the ΔODs are the observed changes in optical density at 690 and 830 nm, and the square-bracketed terms are the resting concentrations of reduced and total hemoglobin from Toricelli et al. (2001). Note that the empirical correction factors cancel and the estimate of relative OEF depends only on the observable quantities and the ratio of baseline concentration values.

Results

Optical recordings

Diffuse optical images reconstructed for five out of the seven subjects showed focal responses (defined as significant change in a subset of source-detector pairs at $P < 0.05$) within the field-of-view of the detection array. In the other two subjects, motion artifacts rendered the signals unusable and no channels were below this significance criterion. Fig. 3 shows group average optical signals, expressed as absolute concentration change, for HbO, HbR, and HbT. Linear model fits for absolute change and baseline values from Toricelli et al. (2001) yielded activation-related response amplitudes of +16 ± 2% for HbO, −13 ± 2% for HbR, and +8 ± 3% for total Hb (changes are expressed as a percentage of the respective baseline concentration for each species).

Arterial spin-labeling

MRI data for all seven subjects showed focal flow responses in the primary motor area, based on maps of t statistic generated for the pooled runs of each subject. Fig. 4 shows ASL-based activation

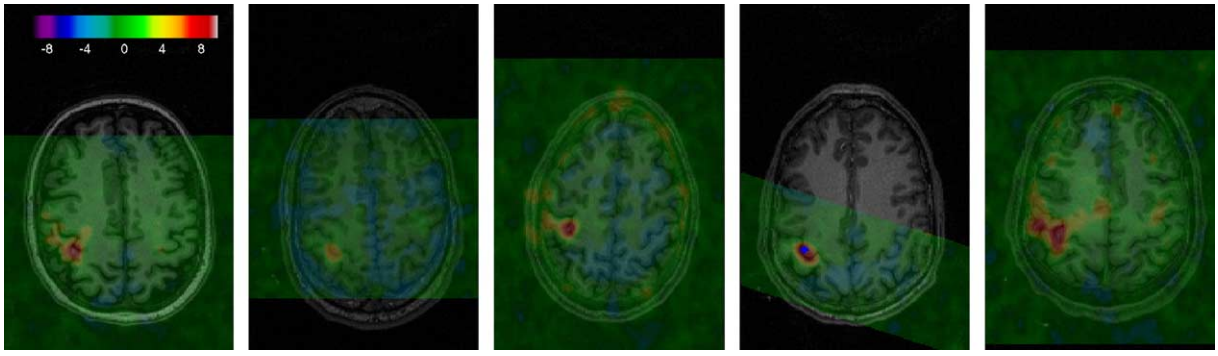

Fig. 4. ASL activation maps. Maps of t statistic overlaid on high-resolution MPRAGE scans are shown for each of the five subjects with usable optical data. The statistical color scale is adjusted so that the $P = 0.01$ threshold corresponds to the transition from green to yellow (for signal increase). Regions of no significant response appear green. Each map shown was generated by mixed effects analysis on all runs for that subject.

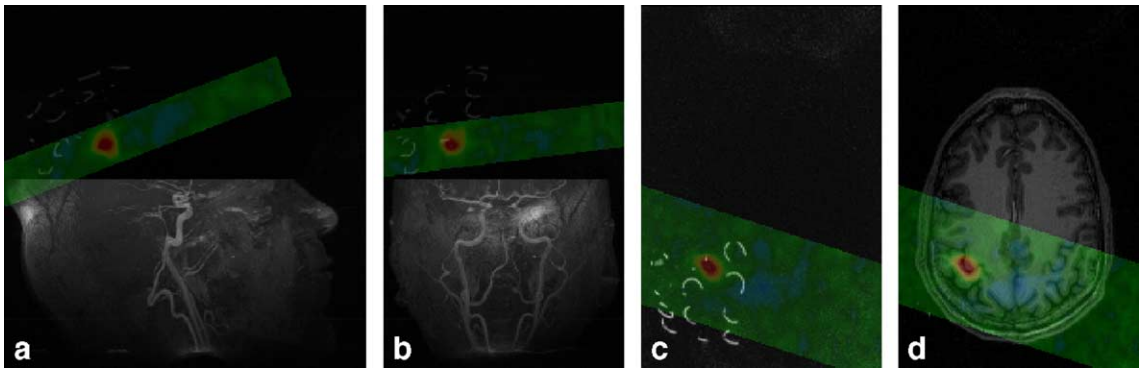

Fig. 5. ASL activation maps superimposed on projections of the source-detector array in one subject. (a) Sagittal view; (b) coronal view; (c) axial view showing only detectors; (d) axial view showing cross-sectional anatomy. In the five subjects used for analysis, the ASL activation focus was within the field-of-view of the optical array.

maps from the five subjects superimposed on their high-resolution structural scans. Fig. 5 shows the ASL activation map for one subject superimposed on a projection of the optical array. Group average flow response amplitudes were computed as described above, yielding an average flow change of +83 ± 9%. The estimated flow response waveform for the group is shown along with optical responses in Fig. 3.

BOLD response

Analysis of the sequence of untagged control images revealed focal BOLD responses in the primary motor cortex contralateral to the hand employed for the task for all subjects. Group average BOLD responses were computed by fitting a linear signal model for the average signals within the same ROI used for ASL, resulting in a group average response of +1.4 ± 0.1%.

$CMRO_2$ estimation

Substitution of optical signals into Eq. (3) allowed estimation of the response waveform for oxygen extraction fraction (Fig. 6). Curves were plotted with a range of assumed values for the arteriovenous mean transit time τ. Differences in assumed τ led to shifts in the curve during periods of rapid change in the optical signal due to the temporal derivative term in Eq. (3). The effect was small, however, and did not significantly alter the general character of the response curve.

Substitution of the estimated steady-state optical density changes and flow response into Eq. (4) yielded a $CMRO_2$ change of +47 ± 5% (Fig. 7). The ratio of fractional changes in oxidative metabolism to fractional change in cerebral blood flow, determined purely by the optical data and Eq. (4), was found to be 0.56 ± 0.08.

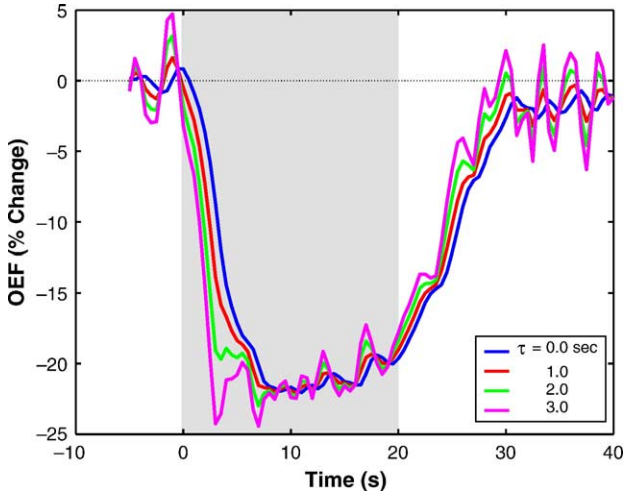

Fig. 6. Plots of percent change in oxygen extraction fraction for different assumed values of arteriovenous transit time τ. The influence of τ is greatest during periods where there is a high rate of change in the optical signals, which lasted approximately 10 s following initiation and cessation of the task.

Discussion

The results demonstrate the feasibility of performing multimodal recordings of physiological responses during functional brain activation and the use of these to compute the cerebral rate of metabolic oxygen consumption. While the specific increase in $CMRO_2$ seen in a particular study is a somewhat arbitrary outcome depending on stimulus intensity and baseline conditions, the ratio of $\Delta\%CMRO_2$:$\Delta\%CBF$ has emerged as a relatively invariant

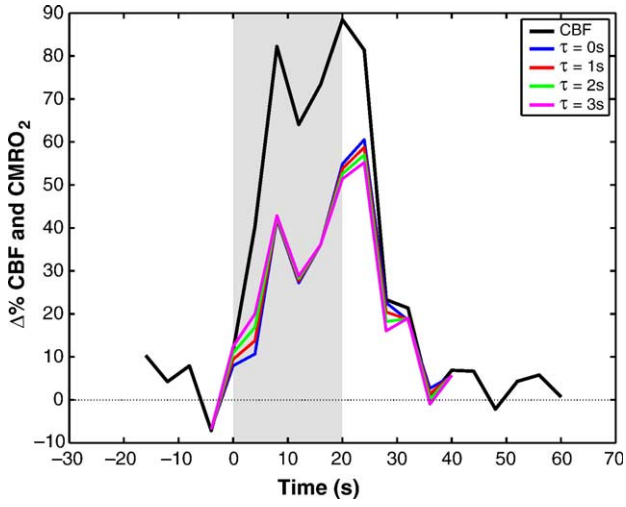

Fig. 7. Plots of percent change for cerebral blood flow and estimated metabolic rate of O_2 consumption. The CMRO2 plots were generated by multiplying the CBF signal by the plots of OEF for different τ shown in figure. The impact of uncertainty in τ is relatively small.

characteristic of cerebrovascular physiology in healthy human brain. The ratio of 0.56 ± 0.08 obtained in the present study based on the observed changed in optical density falls within the range of values seen in previous studies of visual (Hoge et al., 1999b) and motor cortices (Kastrup et al., 2002).

Multimodal observations such as those made in the present study may also allow assessment of the assumptions used in previous uni-modal techniques (Hoge et al., 1999a, 1999b; Kastrup et al., 2002). For example, the apparent increase in cerebral blood volume during activation, as indicated by the optical data, was 8 ± 3%. This is significantly smaller than the value of 26 ± 3% obtained by applying Grubb's relationship (Grubb et al., 1974) to the ASL-based flow change of 83 ± 9%. The absolute accuracy of optically-derived fractional change values is uncertain, however, because these depend on partial-volume correction factor, the differential path length factor, and the values for baseline concentration obtained through prior publications.

In future studies, we hope to remove the need for assumed baseline values in optically-derived quantities by using time-domain optical measurements which, in conjunction with cortically constrained reconstruction methods, will permit computation of absolute baseline concentrations for oxygenated and deoxygenated hemoglobin (Bamett et al., 2003). This should lead to further refinement of the quantitative accuracy of such experiments, particularly in pathological cases where typical baseline physiological parameters may not be applicable.

Note that the estimated fractional change in $CMRO_2$ has fewer dependencies on assumed quantities, as the correction factors cancel in Eq. (4) and the term for relative OEF depends only on the observed changes in optical density and the ratio between baseline values for [HbR] and [HbO]. It is reasonable to expect that at least some sources of systematic error pertaining to the use of literature baseline values are likely to cancel when their ratio is taken. It should also be pointed out that the value reported here for the ratio $\Delta\%CMRO_2$:$\Delta\%CBF$ depends purely on the optical measurements. The ASL-based flow response is used only to scale this ratio into an estimate of fractional change in metabolism.

A final potential confound that should be noted is that the optical and MRI observations made in this study may in general reflect changes over different volumes of brain tissue. However, the response amplitudes presented here reflect average changes over large, diffuse areas of activation that in general appeared at least to overlap. In future studies, we hope to exploit improvements in the optical spatial resolution to better compare apparent spatial extents.

Conclusions

We have used optical measurements of hemoglobin concentration and MRI-based flow imaging to estimate the fractional changes in blood flow and oxidative metabolism during brain activation associated with a motor task. While the combination of optically measured hemoglobin concentrations and MRI-based flow imaging removes some of the assumptions required in single-modality methods, some assumptions were necessary in the present approach. Future studies will be augmented by time-domain optical measurements of baseline hemoglobin concentration and cortically constrained reconstruction of functionally induced optical response patterns.

The ability to record the basic hemodynamic parameters of blood, oxygenation, and volume provides a detailed measure of the quantitative events accompanying neuronal activation that has not previously been available via non-invasive methods in humans. Application of this approach may allow characterization of normal and abnormal response patterns in health and disease, as well as elucidation of the physiological factors shaping temporal response profiles. For example, this method could be employed to investigate whether commonly observed phenomena such as the initial "overshoot" and post-stimulus undershoot in the BOLD signal are caused by a delayed increase in cerebral blood volume (Mandeville et al., 1999).

Acknowledgments

Carsten Warmuth and Kathy Scott are gratefully acknowledged for their assistance in optimizing arterial spin-labeling sequences. We would also like to thank Gary Boas and Dirk Grebert for helping to organize and run experimental sessions. R.J.M.C. is funded by the Brazilian governmental agencies FAPESP and CAPES. T.H. is funded by the Howard Hughes Medical Institute pre-doctoral fellowship program. R.D.H. is funded by the National Institutes of Health (R01RR14543 A01), the MIND Institute, and the Office of National Drug Control Policy. D.A.B. and M.A.F. are funded by the National Institutes of Health (R01-EB002482, P41-RR14075).

References

Bamett, A., Culver, J., Sorensen, A., Dale, A., Boas, D., 2003. Robust inference of baseline optical properties of the human head with three-dimensional segmentation from magnetic resonance imaging. Appl. Opt. 42 (16), 3095–3108.

Boas, D.A., Gaudette, T., Strangman, G., Cheng, X., Marota, J.J.A., Mandeville, J.B., 2003. The accuracy of near infrared spectroscopy and imaging during focal changes in cerebral hemodynamics. Psychophysiology 40 (4), 548–560.

Buxton, R., Wong, E., Frank, L., 1998. Dynamics of blood flow and oxygenation changes during brain activation: the balloon model. Magn. Reson. Med. 6 (39), 855–864.

Davis, T., Kwong, K., Weisskoff, R., Rosen, B., 1998. Calibrated functional mri: mapping the dynamics of oxidative metabolism. Proc. Natl. Acad. Sci. 95 (4), 1834–1839.

Detre, J.A., Alsop, D.C., 2000. Perfusion fMRI with Arterial Spin Labeling. Springer-Verlag, Berlin, pp. 47–61.

Franceschini, M., Fantini, S., Thompson, J., Culver, J., Boas, D., 2001. Hemodynamic evoked response of the sensorimotor cortex measured noninvasively with near-infrared optical imaging. Neuroimage 13 (1), 76–90.

Gratton, G., Maier, J.S., Fabiani, M., Mantulin, W.W., Gratton, E., 1994. Feasibility of intracranial near-infrared optical scanning. Psychophysiology 2 (31), 211–215.

Grubb, R., Phelps, M., Eichling, J., 1974. The effects of vascular changes in $PaCO_2$ on cerebral blood volume, blood flow and vascular mean transit time. Stroke 5, 630–639.

Hoge, R., Atkinson, J., Gill, B., Crelier, G., Marrett, S., Pike, G., 1999a. Investigation of bold signal dependence on cerebral blood flow and oxygen consumption: the deoxyhemoglobin dilution model. Magn. Reson. Med. 42 (5), 849–863.

Hoge, R., Atkinson, J., Gill, B., Crelier, G., Marrett, S., Pike, G., 1999b. Linear coupling between cerebral blood flow and oxygen consumption in activated human cortex. Proc. Natl. Acad. Sci. 96 (16), 9403–9408.

Jobsis, F.F., 1977. Noninvasive infrared monitoring of cerebral and

myocardial sufficiency and circulatory parameters. Science 4323 (198), 1264–1267.
Kastrup, A., Kruger, G., Neumann-Haefelin, T., Glover, G., Moseley, M., 2002. Changes in cerebral blood flow, oxygenation, and oxidative metabolism during graded motor activation. Neuroimage 15 (1), 74–82.
Kim, S., Ugurbil, K., 1997. Comparison of blood oxygenation and cerebral blood flow effects in fmri: estimation of relative oxygen consumption change. Magn. Reson. Med. 38 (1), 59–65.
Kim, S.G., 1995. Quantification of relative cerebral blood flow change by flow-sensitive alternating inversion recovery (FAIR) technique: application to functional mapping. Magn. Reson. Med. 34 (3), 293–301.
Kwong, K.K., Belliveau, J.W., Chesler, D.A., Goldberg, I.E., Weisskoff, R.M., Poncelet, B.P., Kennedy, D.N., Hoppel, B.E., Cohen, M.S., Turner, R., 1992. Dynamic magnetic resonance imaging of human brain activity during primary sensory stimulation. Proc. Natl. Acad. Sci. 89 (12), 5675–5679.
Luh, W., Wong, E., Bandettini, P., Hyde, J., 1999. QUIPSS II with thin-slice ti1 periodic saturation: a method for improving accuracy of quantitative perfusion imaging using pulsed arterial spin labeling. Magn. Reson. Med. 6 (41), 1246–1254.
Mandeville, J., Marota, J., Ayata, C., Zaharchuk, G., Moskowitz, M., Rosen, B., Weisskoff, R., 1999. Evidence of a cerebrovascular postarteriole windkessel with delayed compliance. J. Cereb. Blood Flow Metab. 19 (6), 679–689.
Ogawa, S., Tank, D.W., Menon, R., Ellermann, J.M., Kim, S.G., Merkle, H., Ugurbil, K., 1992. Intrinsic signal changes accompanying sensory stimulation: functional brain mapping with magnetic resonance imaging. Proc. Natl. Acad. Sci. 89 (13), 5951–5955.
Sfareni, R., Boffi, A., Quaresima, V., Ferrari, M., 1997. Near infrared absorption spectra of human deoxy- and oxyhaemoglobin in the temperature range 20–40 degrees C. Biochim. Biophys. Acta 2 (1340), 165–169.
Strangman, G., Franceschini, M., Boas, D., 2003. Factors affecting the accuracy of near infrared spectroscopy concentration calculations for focal changes in oxygenation parameters. Neuroimage 4 (18), 865–879.
Toricelli, A., Pifferi, A., Taroni, P., Giambattistelli, E., Cubeddu, R., 2001. In vivo optical characterization of human tissues from 610 to 1010 nm by time-resolved reflectance spectroscopy. Phys. Med. Biol. 46, 2227–2237.
Villringer, A., Chance, B., 1997. Non-invasive optical spectroscopy and imaging of human brain function. Trends Neurosci. 20 (10), 435–442.
Wong, E., Buxton, R., Frank, L., 1997. Implementation of quantitative perfusion imaging techniques for functional brain mapping using pulsed arterial spin labeling. NMR Biomed. 4–5 (10), 237–249.
Worsley, K., Friston, K., 1995. Analysis of fmri time-series revisited—again. Neuroimage 3 (2), 173–181.
Wray, S., Cope, M., Delpy, D.T., Wyatt, J.S., Reynolds, E.O., 1988. Characteristics of the near infrared absorption spectra of cytochrome aa3 and hemoglobin for noninvasive monitoring of cerebral oxygenation. Biochim. Biophys. Acta 1 (933), 184–192.